Novel multi-transmitter calyx-like giant synapse revealed in the extended amygdala

Limei Zhang[1, 2†,10*], Vito S. Hernández[1, 2†,10], David M. Giraldo[3, 4], Juan C. León-Contreras[5], Rong Ye[6], Shiliang Zhang[6], Martin K-H Schäfer[7], Rafael A. Barrio[8], Rogelio Hernández-Pando[5], Francesco Ferraguti[9] and Lee E. Eiden[2],

[1]Department of Physiology, School of Medicine, National Autonomous University of Mexico

[2]Section on Molecular Neuroscience, National Institute of Mental Health, NIH, USA.

[3]Microscopy Core, School of Medicine, National Autonomous University of Mexico, Mexico City Mexico.

[4] ZEISS Innovation Center, Dublin, California, USA

[5]Department of Experimental Pathology, National Institute of Medical Sciences and Nutrition, Mexico

[6]Confocal and Electron Microscopy Core, National Institute on Drug Abuse, NIH, USA.

[7]Institute of Anatomy and Cell Biology, Philipps University Marburg, Marburg, Germany.

[8]Department of Complex Systems, Institute of Physics, UNAM, Mexico.

[9]Institute of Pharmacology, Medical University of Innsbruck, Innsbruck, Austria.

[10]Equal contribution

[†]Sabbatical researcher

*Correspondence: limei@unam.mx

Abstract: The calyx of Held, a giant excitatory cup-like axo-somatic synapse, has been historically described exclusively in the auditory brainstem. Here, using PACAP immunohistochemistry combined with confocal and tomographic electron microscopy, we report the discovery of a morphologically similar calyx-like synapse in the extended amygdala of rodents, exhibiting unique neurochemical features. This previously unrecognized structure forms massive axo-somatic terminals with mixed glutamatergic and cholinergic identities, co-expressing VGluT1, VGluT2, VAChT, and the neuropeptides PACAP, CGRP, and neurotensin, along with calretinin in the presynaptic compartment. The postsynaptic targets are a distinct subset of PKCδ-expressing neurons that co-express the synaptic adhesion molecule GluD1. Strikingly, GluD1 immunolabeling is concentrated specifically at axo-somatic contact sites apposed to VAChT+ calyceal terminals, but absent at PSD of conventional type I synapse, suggesting a specialized molecular architecture for calyceal synapse. Our findings reveal a previously unknown calyx-like synapse in the forebrain, exhibiting a unique convergence of fast and modulatory transmission with implications for transmission fidelity within emotional-viscerosensory circuits.

Significance Statement: Fast and reliable excitatory transmission is essential for neural circuits that govern rapid sensory processing. Until now, the calyx of Held synapse was the only known giant axo-somatic glutamatergic terminal in the mammalian brain. Here, we identify a previously unrecognized calyx-like synapse in the extended amygdala, a key center for emotional and autonomic integration. This massive, multimodal synapse combines glutamatergic, cholinergic, and peptidergic transmission and targets a distinct subset of PKCδ neurons. Its molecular composition, including VGLUT1/2, VAChT, PACAP, and GluD1, suggests a unique structural and functional specialization. This discovery broadens our understanding of synaptic diversity and reveals a novel anatomical substrate for high-fidelity communication in emotional-viscerosensory circuits.

key words: Calyx of Held, axo-somatic synapse, FEBSEM, TEM, multitransmitters, co-transmission, neuropeptides, GluD1, PKCδ

Introduction

Precise and high-fidelity neurotransmission is a hallmark of certain specialized synaptic architectures in the mammalian brain. One of the most striking examples is the calyx of Held, a giant axo-somatic glutamatergic terminal in the auditory brainstem (Nakamura and Cramer 2011), first described over a century ago by Hans Held (Held 1893). This unique synapse, formed by globular bushy cells onto principal neurons in the medial nucleus of the trapezoid body (MNTB), is characterized by its expansive presynaptic terminal that engulfs the soma of its postsynaptic target, supporting fast, one-to-one spike transmission with minimal delay and jitter (Satzler, Sohl et al. 2002, Lorteije, Rusu et al. 2009, Nakamura and Cramer 2011). The structure and function of the calyx of Held have provided a foundational model for understanding synaptic reliability, vesicle dynamics, and temporal precision in sensory circuits.

While some features of calyx synapses have been observed in hippocampal mossy fiber boutons and cerebellar climbing fiber terminals (Harris and Weinberg 2012), they predominantly target dendrites and lack the fully enveloping, axo-somatic morphology of the calyx of Held. Similarly, some early works reported neuropeptide calcitonin gene-related peptide (CGRP)-expressing large synaptic boutons forming axo-somatic synapses that, however, did not report to encircle the postsynaptic neurons (Shimada, Shiosaka et al. 1985, Dong, Fukazawa et al. 2010). Therefore, no such calyx-like fast relay synapses have been described in forebrain circuits, so far.

The central amygdala (CeA) and bed nucleus of the stria terminalis (BST) serve as crucial hubs for rapid viscerosensory processing and for coordinating autonomic, behavioral, and emotional responses to threats and homeostatic challenges. These interconnected nuclei receive robust brainstem inputs carrying visceral and nociceptive information – notably from the parabrachial nucleus (PBN) – which alert the extended amygdala to internal bodily states and imminent threats (Takeuchi, Xie et al. 2004, Jaramillo, Brown et al. 2021). In turn, the CeA and BNST project to hypothalamic and brainstem effectors to orchestrate fear and stress responses. For example, the CeA is well known to drive defensive behaviors (like freezing and startle) and autonomic adjustments (such as changes in heart rate and stress hormone release) during conditioned fear, via its projections to the brainstem and hypothalamus (Radke 2009).

In the course of characterizing PACAPergic projections to the extended amygdala, we serendipitously discovered ring-like axo-somatic structures in the capsular subdivision of the CeA (CeC) and in the oval nucleus of the BST (ovBST). These structures, revealed by immunohistochemistry for PACAP, exhibited a morphology reminiscent of the calyx of Held. Using a combination of confocal microscopy, electron tomography (focused ion beam scanning electron microscopy, FIBSEM), and 3D reconstructions, we report here that these are indeed massive calyx-like terminals forming multiple synaptic contacts on the soma of a distinct PKCδ-expressing neuronal population. Remarkably, these terminals exhibit a multimodal transmitter identity, co-expressing the vesicular glutamate transporter 1 and/or 2 (VGluT1 and/or VGlut2),

vesicular acetylcholine transporter (VAChT), along with the neuropeptides PACAP, CGRP and neurotensin, as well as the calcium binding protein calretinin. Their postsynaptic targets besides PKCδ, express GluD1, a synaptic adhesion molecule previously implicated in the stabilization of large glutamatergic synapses (Dai, Patzke et al. 2021, Liakath-Ali, Polepalli et al. 2022), suggesting the integration of excitatory, cholinergic, and peptidergic signaling at this site. Collectively, our findings uncover previously unknown calyx-like synapses in the forebrain, exhibiting a unique convergence of fast and modulatory transmission, with implications for the structural logic of high-fidelity signal integration in viscerosensory-affective circuit.

Results

To assess the distribution of PACAPergic inputs in the rat telencephalon, we performed immunohistochemistry and identified a highly selective ring-like innervation pattern in distinct forebrain regions. These perisomatic PACAP-positive structures were especially prominent in the CeC, the ovBST, and, to a lesser extent, scattered within the dorsal and ventral subdivisions of the lateral septal nucleus (see Supplemental Fig. 1).

Within the amygdaloid complex (Fig. 1A–B), we observed heterogeneous PACAP immunoreactivity across multiple nuclei. A dense mesh of fine, varicose PACAP-immunoreactive (PACAP-ir) fibers was distributed in regions such as the lateral amygdala (LA, Fig. 1B2), postero-dorsal medial amygdala (MePD, Fig. 1B4), posteroventral medial amygdala (MePV), basolateral (BLA), and basomedial (BMA, Fig. 1B3) amygdala, as well as in the central lateral (CeL) and central medial (CeM) subdivisions—forming diffuse en passant-type innervation patterns. In contrast, the CeC displayed a population of thicker, non-varicose PACAP+ fibers forming distinct ring-like axo-somatic arrangements around a subpopulation of neurons (Fig. 1A and B1, arrows), particularly enriched in its posteroventrolateral region.

To determine the postsynaptic target of these PACAPergic rings, we first assessed somatostatin (SST)-expressing neurons, but these lacked expression of the PAC1 receptor. Since both the CeC and ovBST are known to also contain a high density of PKCδ-expressing neurons (Daniel and Rainnie 2016), we then examined PKCδ-expressing neurons, the other main cell population in the CeC. To visualize them, we used Prkcd-Cre::Ai9 double transgenic mice, in which PKCδ+ neurons are fluorescently labeled with tdTomato. In horizontal sections of the CeC (Fig. 1C), PACAP+ fibers (green) formed perisomatic rings around tdTomato+ PKCδ neurons (red). This was especially prominent in the caudal CeC (Fig. 1C1). As shown in Fig. 1 (Fig. 1D), PACAP-ir appeared juxtaposed to GluD1 immunolabeled structures aligned with the somatic plasma membrane of tdTomato+ cells, supporting a direct axo-somatic PACAPergic input onto PKCδ+ neurons.

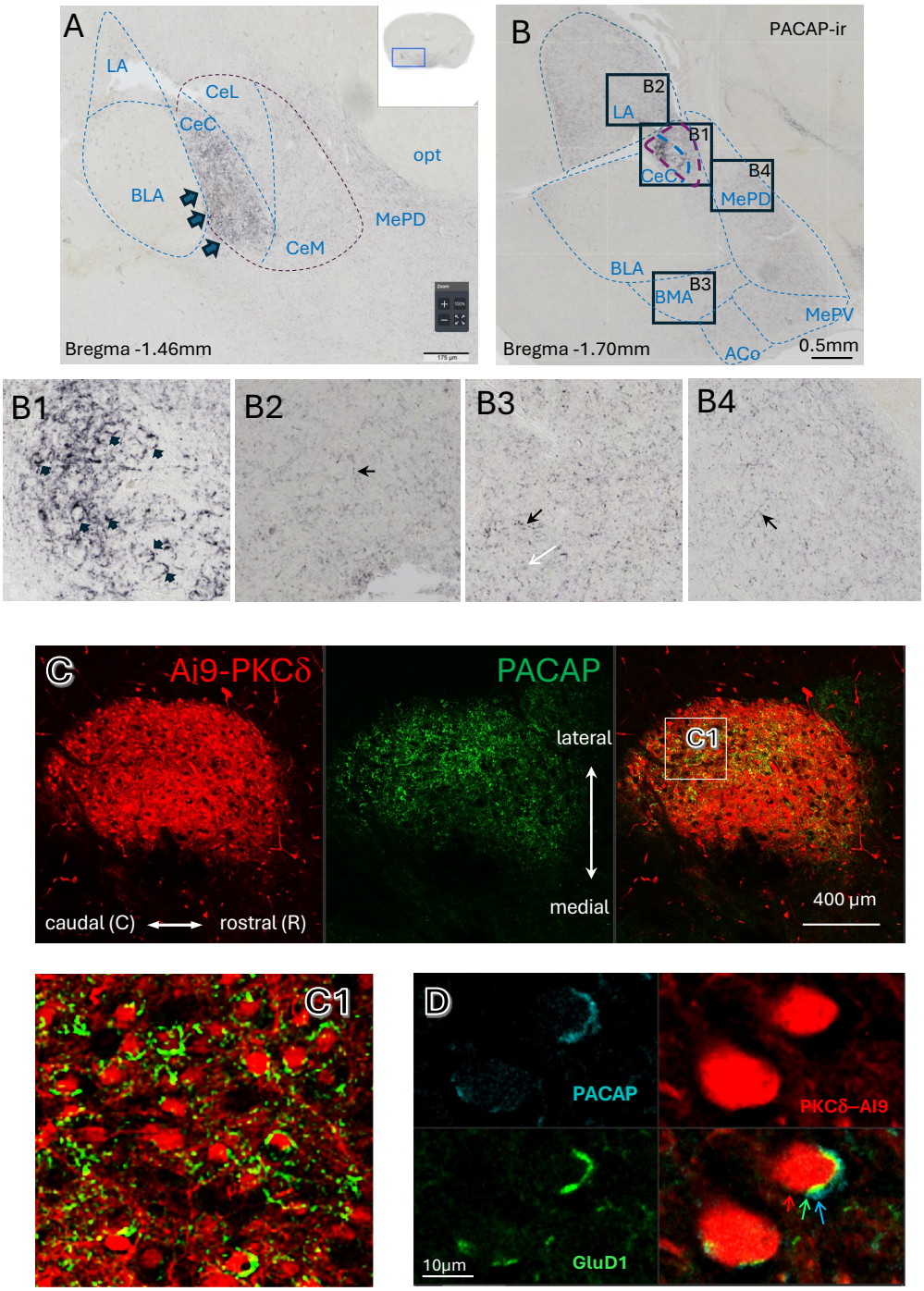

Figure 1. PACAP+ fibers form perisomatic ring-like innervation patterns targeting PKCδ+ neurons in the capsular central amygdala. (A–B) Coronal sections of the rat amygdaloid complex showing PACAP-immunoreactive (PACAP-ir) fiber distribution. Blue dashed outlines mark amygdaloid nuclei; CeC = capsular central amygdala; CeL = lateral central; CeM = medial central; BLA = basolateral; BMA = basomedial; LA = lateral amygdala; MePD/MePV = posterodorsal/posteroventral medial amygdala. Insets B1–B4 show regional fiber morphologies (arrows in B1 indicate PACAP+ perisomatic rings in the CeC). (C) Horizontal section from a Prkcd-Cre::Ai9 mouse showing tdTomato-labeled PKCδ+ neurons (red) and PACAP immunostaining (green) in the CeC. (C1) High-magnification image of the caudal CeC reveals PACAP+ perisomatic rings around PKCδ+ cells. (D) High-resolution immunostaining for PACAP,

GluD1, and tdTomato shows PACAP labeling surrounding PKCδ+ cell bodies (red), with GluD1 signal (green) localized to membrane segments in close apposition to PACAP+ structures.

To determine the postsynaptic response of PKCδ-expressing neurons in the CeC to PACAP, we performed ex vivo whole-cell patch-clamp recordings in brain slices obtained from Prkcd-Cre::Ai9 mice, in which PKCδ+ neurons are labeled with tdTomato. Recordings were conducted in artificial cerebrospinal fluid (ACSF), with a 100 nM PACAP bath application and subsequent washout (Fig. 2A).

Electrophysiological analysis revealed the presence of two distinct neuronal subtypes based on their response to PACAP. Type 1 neurons (red symbols, Fig. 2A–C) showed a robust and reversible increase in action potential firing frequency during PACAP application (Fig. 2B), accompanied by a slope increase in the current–frequency (I–F) response curve (Fig. 2C), indicating enhanced excitability.

Post hoc immunohistochemical analysis of these PACAP-sensitive cells revealed plasma membrane expression of GluD1 (Fig. 2D, left panel), and their cellular morphology was confirmed through biocytin filling (Fig. 2D, right panel). These features are consistent with the perisomatically innervated PKCδ+ neurons described in Figure 1.

In contrast, Type 2 neurons (blue symbols, Fig. 2E–F) exhibited no significant change in firing frequency during PACAP application. These PACAP-insensitive neurons lacked GluD1 membrane localization, despite also being tdTomato+ (Fig. 2F). Their identity and morphology were likewise confirmed via biocytin labeling (Fig. 2F, right panel).

These results support the existence of functionally and molecularly distinct subtypes of PKCδ+ neurons in the CeC, with differential sensitivity to PACAP and selective expression of GluD1.

Figure 2. Whole-cell recordings reveal PACAP-sensitive and -insensitive subtypes of PKCδ+ neurons in the central amygdala.

(A) Schematic of ex vivo patch-clamp recordings in horizontal brain slices from Prkcd-Cre::Ai9 mice, showing tdTomato+ PKCδ neurons in the CeC. (B) Representative current-clamp traces from a Type 1 neuron showing increased firing in response to PACAP (100 nM, red), reversible upon washout (blue). (C) I–F curve showing increased excitability in Type 1 neurons during PACAP application (red curve, red crosses).
(D) Post hoc analysis of the same Type 1 cell showed GluD1 expression (cyan) localized to the plasma membrane (left), and biocytin labeling of dendritic morphology (right).
(E–F) Type 2 neurons (blue crosses) showed no change in firing rate in response to PACAP (F).
(G) These PACAP-insensitive PKCδ+ neurons lacked GluD1 membrane expression (left), despite successful biocytin filling (right). Scale bars: 10 μm (D, G left); 50 μm (D, G right).

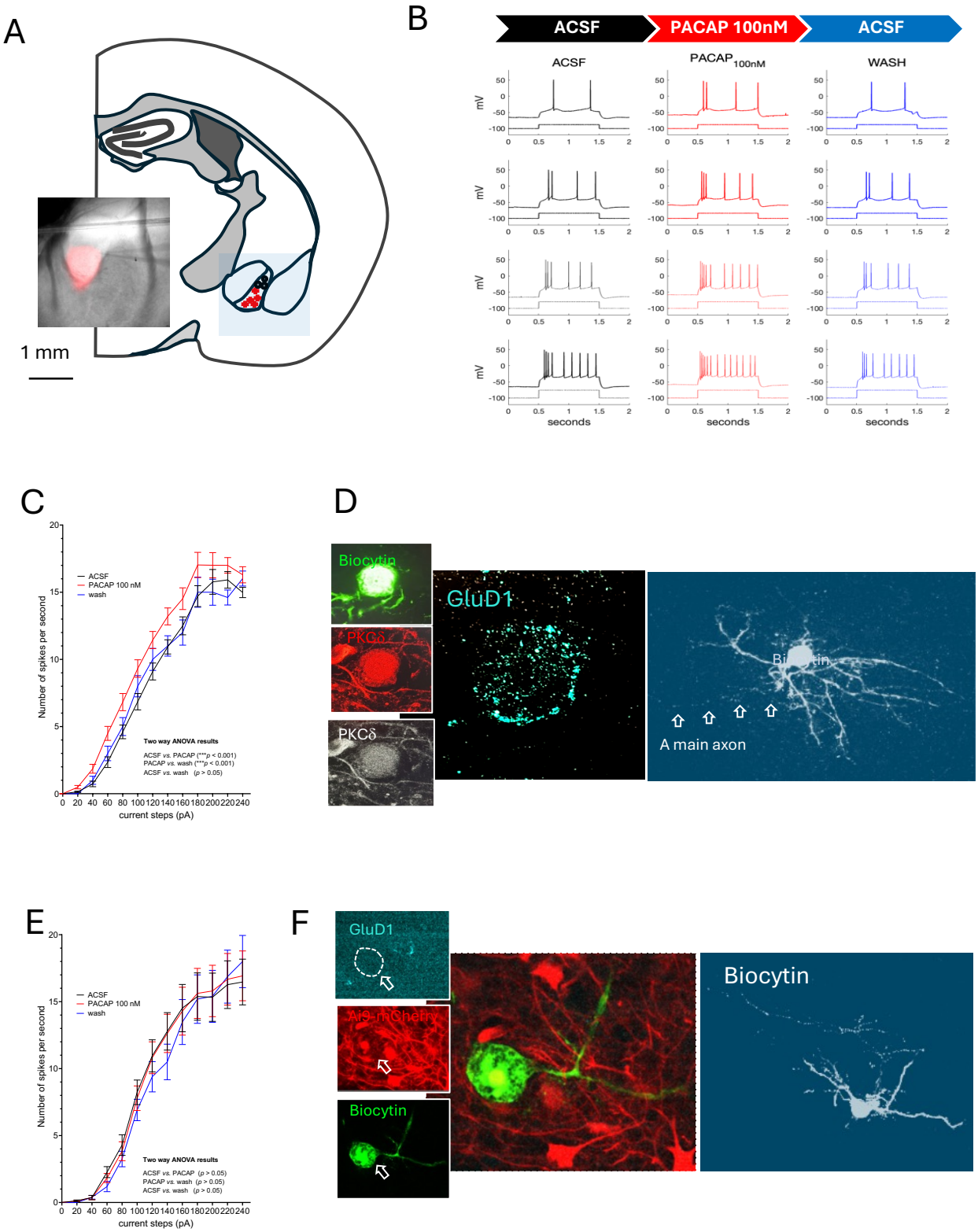

Figure 2 (caption in the previous page)

We then decided to delve further into the molecular architecture of these large perisomatic PACAP+ terminals. High-resolution confocal imaging revealed that these ring-like axon terminals co-expressed the vesicular glutamate transporter 1 (VGLUT1) and/or 2 (VGLUT2) (Fig. 3, panel D, A11, 12, A17, B6 y B7 and Fig. 5 panel H, at electron microscopy level), analogously to the calyx of Held in the medial nucleus of trapezoid body (MNTB), and the vesicular acetylcholine transporter VAChT (Fig. 3, panels B). Furthermore, the presynaptic PACAP+ rings around the somata of PKCδ-expressing neurons contained the neuropeptides calcitonin-gene related peptide (CGRP) and neurotensin, as well as the calcium binding protein calretinin (Fig. 3, panels C). These findings indicate a multimodal transmitter phenotype for these axon terminals that include glutamatergic, cholinergic, and peptidergic components. To prove that their spatial organization is similar to that of a calyx of Held (calyx-like), we performed confocal z-stacks of PKCδ-expressing neurons segmentation in the CeC. The PACAP+ fibers formed large cup-like, enveloping axo-somatic terminals, confirming their calyx-like macro-architecture (Fig. 3, D).

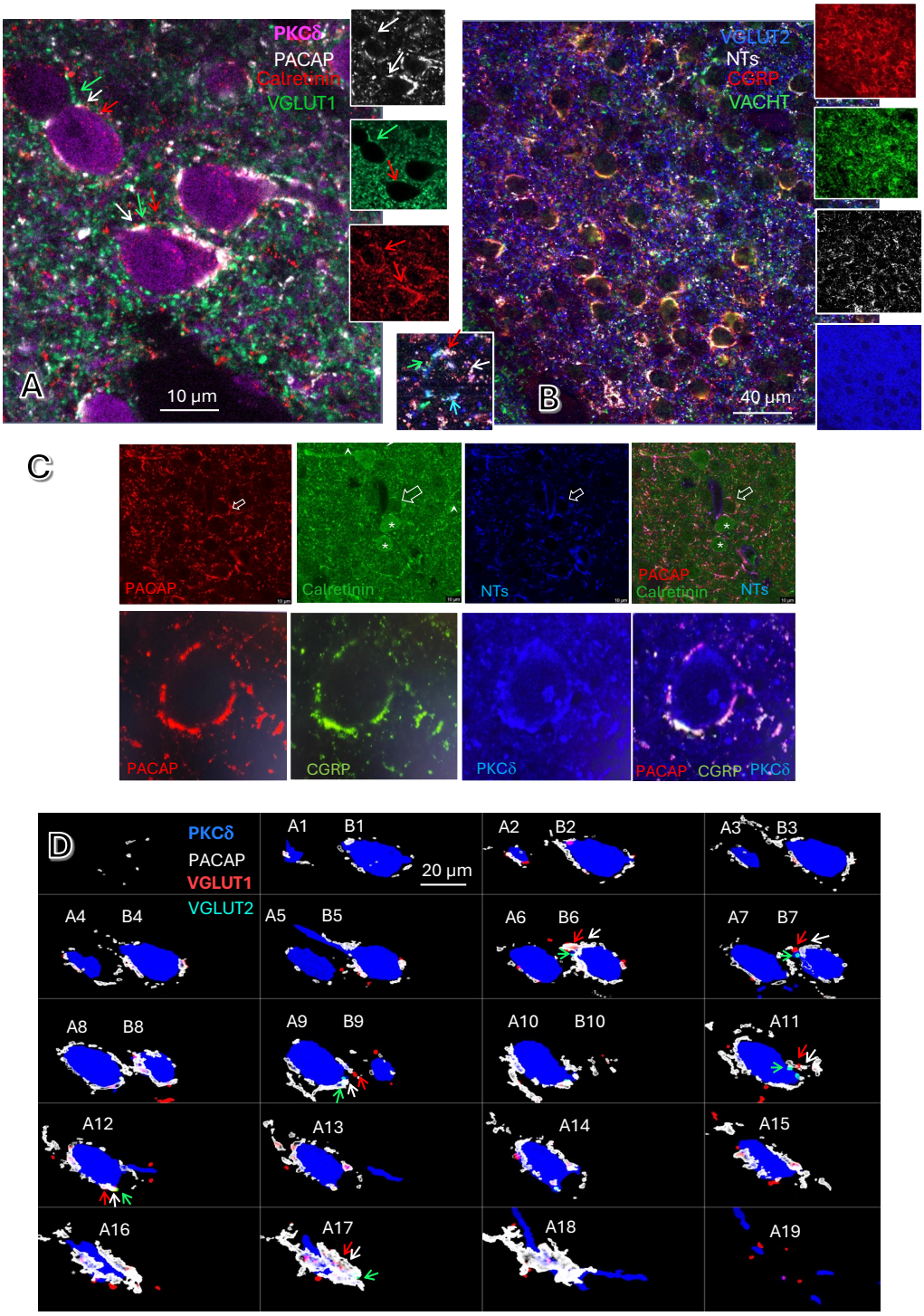

Figure 3: Neurochemical composition of the ring-like structure in the CeC:

A. B: High-magnification views demonstrate that these perisomatic structures co-express multiple markers, including in A: VGLUT1 (green arrows), calretinin (red arrows), PACAP (white arrows), in B: neurotensin (white arrow in D), vesicular acetylcholine transporter (VAChT, green arrow in D), VGLUT2 (cyan arrow in D), and calcitonin gene-related peptide (CGRP, red arrow).

C: the co-expression of neuropeptides (neurotensin, Nts), CGRP and calcium binding protein calretinin with PACAP+ ring-like structure engulfing PKCd positive cell body.

D. Segmentation of 20 serial confocal optical sections of two PKCδ-expressing neurons (blue) illustrates the spatial organization of the ring-like fibers around the somata within the CeC.

To study the ultrastructural organization of these PACAP+ calyx-like structures, we employed focused ion beam-scanning electron microscopy (FIB-SEM) combined with immunoelectron labeling. Analysis of two serial sections (n = 450 and 240) from a DAB-labeled sample of the rat CeC revealed giant PACAP+ terminals encapsulating postsynaptic somata and exhibiting a dense network of synaptic contacts, fully consistent with a calyx of Held-like morphology (Fig. 4 and supplementary videos 1-3).

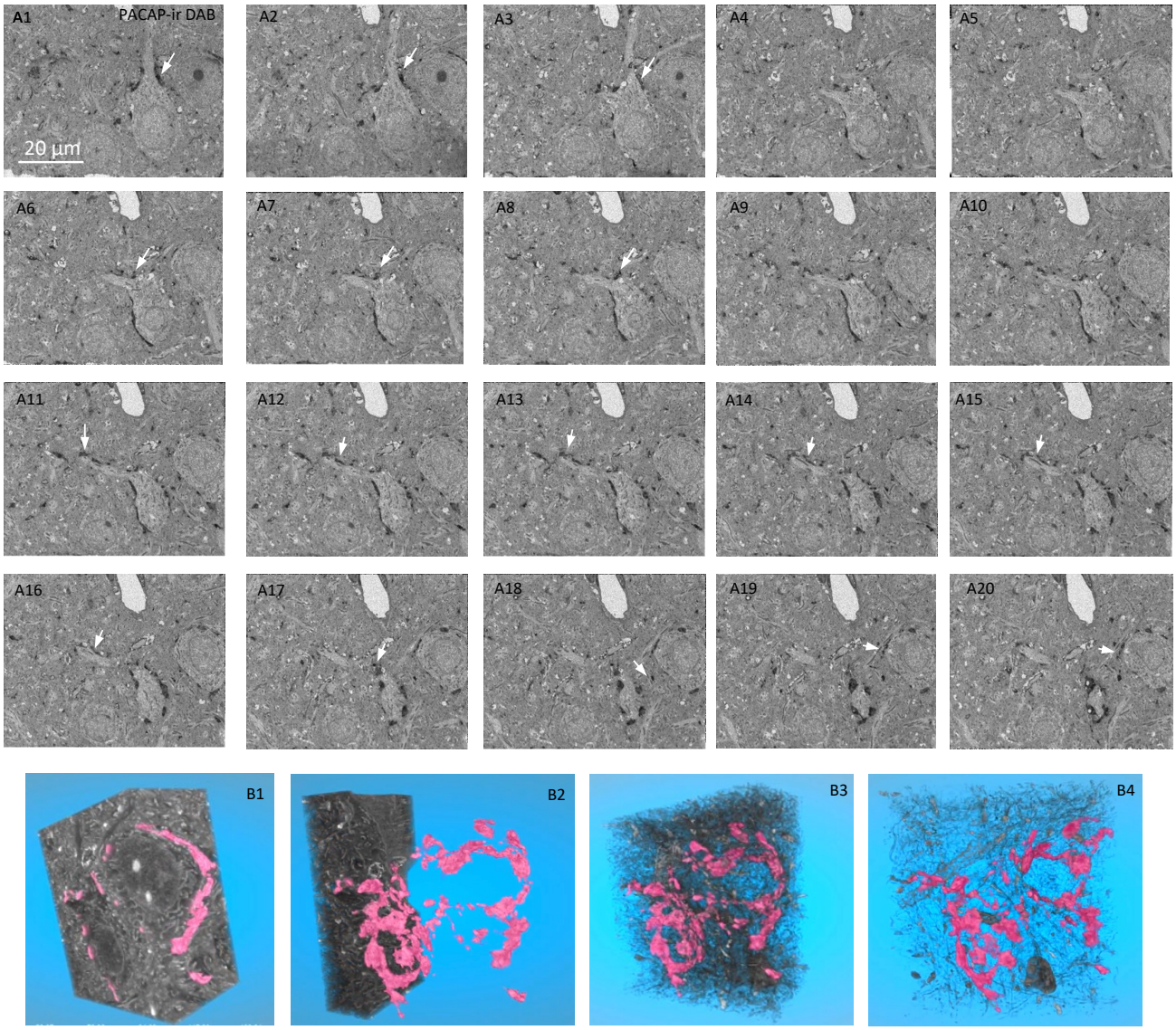

Figure 4. A calyx of Held-like, ring-shaped synaptic structure in the central amygdala (CeC-calyceal synapse) revealed by tomographic electron microscopy.

Panels A1–A18: Selected frames from a series of 450 FIB-SEM (Focused Ion Beam Scanning Electron Microscopy) images from an immunoelectron microscopy sample labeled with rabbit anti-PACAP antibody and visualized using a peroxidase-DAB reaction. These frames illustrate the sequential progression of two PACAP-positive calyceal synapses.

Panels B1–B4: 3D reconstruction and segmentation of the same sample highlighting the ring-like morphology of the PACAP+ calyceal synapses. Corresponding video files showing the full reconstruction are available in the Supplemental Information.

Finally, by leveraging pre-embedding electron microscopy, we revealed that CeC calyx-like synapses exhibit unconventional chemo-anatomical properties. PACAP+ calyceal axons formed both asymmetric (Type I) and symmetric (Type II) synaptic contacts (Fig. 5A), occasionally observed adjacent within the same terminal, but with a higher prevalence of Type II configurations (Fig. 5B). Noteworthy, we often detected strong GluD1 immunometal labeling of the plasma membrane specialization of PKCδ-expressing neurons postsynaptic to the PACAP+ terminals (Fig. 5C), suggesting a specific molecular identity for this synaptic pairing. Cholinergic terminals expressing VAChT also formed GluD1-positive Type II synapses (Fig. 5D), reinforcing the idea that GluD1 expression is closely associated with cholinergic inputs. In contrast, nearby glutamatergic synapses (VGluT1/2-positive) typically exhibited classic asymmetric morphology and lacked GluD1 labeling (Fig. 5E). These findings support the notion that CeC-calyceal synapses represent a specialized subpopulation of central amygdalar connections, distinguished by their molecular profiles and potential neurotransmitter signaling mechanisms.

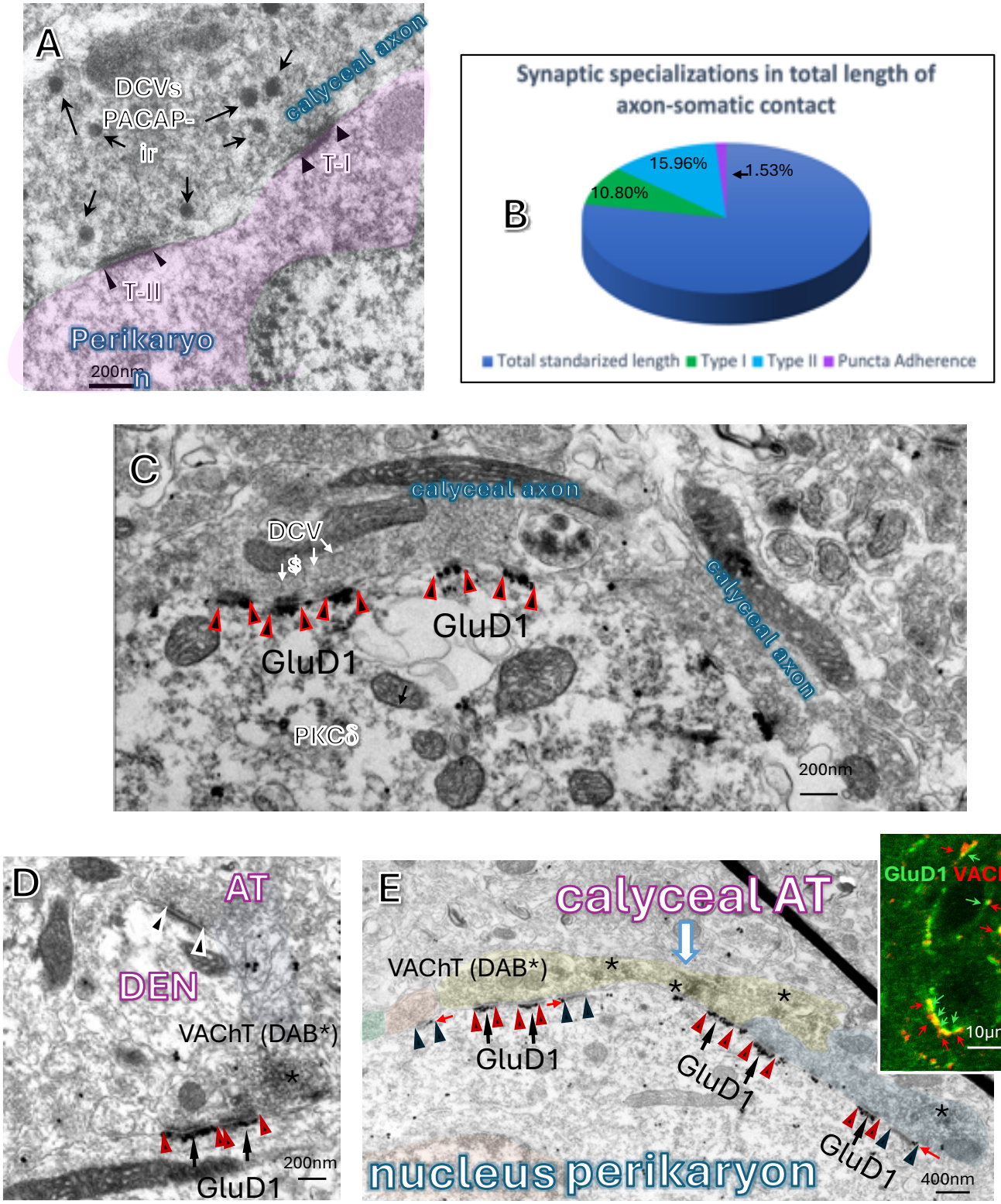
A
DCVs
PACAP-
ir
calyceal axon
T-I
T-II
Perikaryo
200nm
n
B
Synaptic specializations in total length of axon-somatic contact
15.96%
1.53%
10.80%
Total standarized length
Type I
Type II
Puncta Adherence
C
calyceal axon
DCV
GluD1
GluD1
calyceal axon
PKCδ
200nm
D
AT
DEN
VAChT (DAB*)
GluD1
200nm
E
calyceal AT
VAChT (DAB*)
GluD1
GluD1
GluD1
nucleus perikaryon
400nm
GluD1 VAChT
10µm

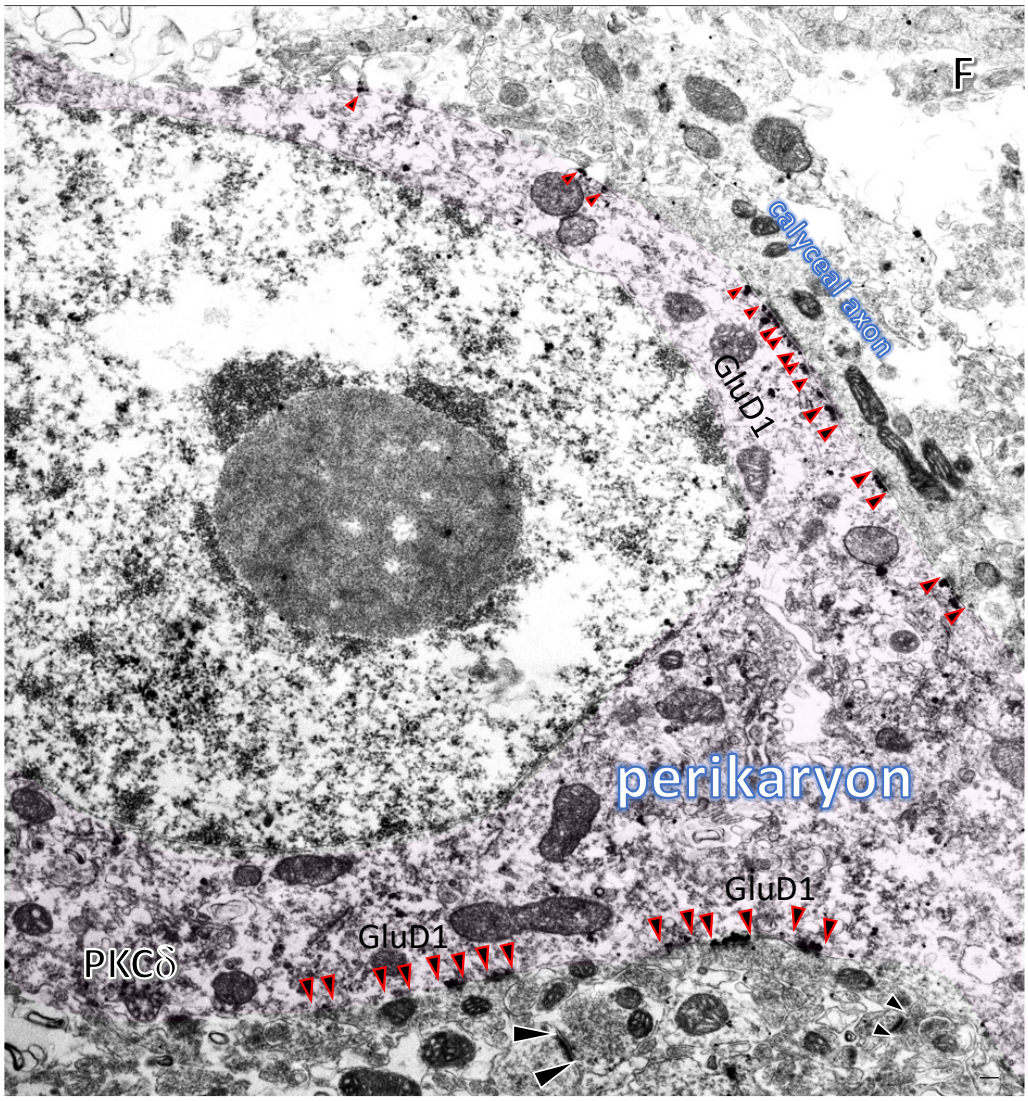
F
calyceal axon
GluD1
perikaryon
GluD1
GluD1
PKCδ

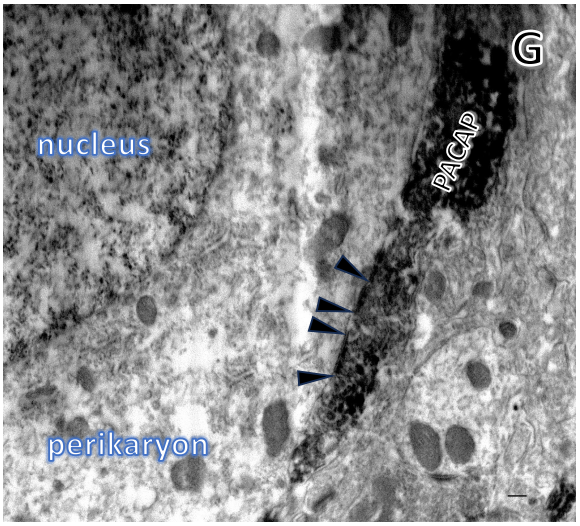
G
nucleus
PACAP
perikaryon

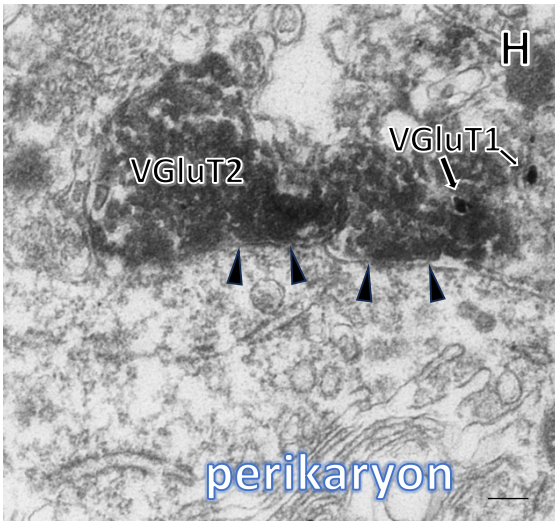
H
VGluT2
VGluT1
perikaryon

Figure 5. The CeC-calyceal synapse exhibits distinct chemoanatomical features.

A. A PACAP-expressing calyceal axon forms both asymmetric (Type I, thick arrowheads) and symmetric (Type II, narrow arrowheads) synaptic contacts. Presynaptic vesicles and both pre- and postsynaptic densities (PSDs) are visible.

B. A pie chart quantifies the proportion of each synapse type based on contact length measurements from randomly selected TEM micrographs (n = 30) in which synaptic specialization could be identified.

C. Double-label immunoelectron microscopy (DAB for PKCδ and immunogold for GluD1) shows a PACAP+ calyceal axon making multiple Type II synapses onto a PKCδ-expressing (DAB-labeled) neuron. The PSDs are densely labeled with GluD1-immunogold particles (red-black bicolored arrowheads). The inset shows a confocal immunofluorescence image where a PACAP+ axon (cyan) surrounds a PKCδ+ soma (red), and GluD1 expression (green) is localized at the interface between them, corresponding to the presumed postsynaptic membrane (indicated by 3-color arrows).

D. A DAB-labeled axon terminal expressing vesicular acetylcholine transporter (VAChT, *) forms a Type II synapse, with dense GluD1-gold particle labeling at the PSD (red-black arrowheads). For comparison, an adjacent unlabeled axon terminal (AT) forms a clear Type I synapse devoid of GluD1 labeling (white-black arrowheads). Inset adapted from Wainer et al. (1984) highlights the typical morphology of central cholinergic synapses, where the active zone shows electron-dense material comparable to the PSD, often resembling symmetric synapses. CHAT: choline acetyltransferase.

E. Another example of a VAChT+ (*) calyceal axon forming Type II synapses with GluD1-gold labeling (black arrows) at the PSDs. Inset: confocal image showing close spatial correspondence between VAChT (red) and GluD1 (green) signals. GluD1 expression is localized between the red VAChT-positive axon and the soma, suggesting a tight anatomo-functional association between cholinergic input and GluD1 expression.

F. A large PKCδ-expressing (DAB-labeled) neuron receives multiple GluD1-positive synaptic contacts (red-black arrowheads) along its soma and proximal dendrite. Two adjacent Type I synapses from unlabeled axons are GluD1-negative (white-black arrowheads), underscoring the specificity of GluD1 labeling to Type II synapses and suggesting a molecular distinction between glutamatergic and cholinergic inputs.

G. and **H** PACAP+ (DAB G) and VGluT1 and VGluT2 co-expressing calyceal axon (H) form multiple synaptic specifications one contacts onto CeC cells.

Discussion

This work represents the first comprehensive morphological evidence for the presence of calyx-like synapses in the forebrain, and suggests a specialized role for PACAP+ neurons in rapid or synchronized signal transmission within central emotional processing circuits.

In this study, we identified a distinct subpopulation of large axo-somatic terminals in the CeC and ovBST, revealed by PACAP immunoreactivity and confirmed by confocal and FIBSEM-based 3D reconstructions. These terminals form massive calyx-like synaptic contacts on PKCδ-expressing neurons that co-express *GluD1*, defining a novel discrete subpopulation of PKCδ-expressing neurons based on unique molecular and anatomical signatures. The presynaptic compartment of these calyceal terminals is neurochemically rich, co-expressing VGLUT1, VGLUT2, VAChT, calretinin, and the neuropeptides PACAP, CGRP, and neurotensin. Extensive EM analysis revealed multiple asymmetric and symmetric synaptic specializations, often aligned with GluD1-immunolabeled postsynaptic domains. Electrophysiological recordings confirmed that PACAP application enhances excitability in CeC PKCδ neurons, suggesting functional engagement of this novel synapse. Collectively, our findings uncover a previously unknown calyceal synapse in the forebrain, exhibiting a unique convergence of fast and modulatory transmission, with implications for the structural logic of high-fidelity signal integration in viscerosensory-affective circuits.

The identification of calyx-like terminals in the CeC and ovBST challenges traditional views of synaptic architecture in the extended amygdala and probably beyond. While calyceal synapses such as the calyx of Held are well characterized in auditory brainstem circuits for their fast, high-fidelity transmission, analogous structures have not previously been described in forebrain regions. The morphology and complexity of the terminals we observed—combined with their molecular signatures—suggest a similar capacity for rapid and synchronized signal delivery, potentially coordinating responses to highly salient visceral or emotional stimuli.

The convergence of classical neurotransmitters (glutamate and acetylcholine) with multiple neuropeptides in the same terminal is particularly noteworthy. This co-transmission strategy implies a capacity for both rapid excitation and longer-lasting modulatory influence on postsynaptic PKCδ neurons. The consistent postsynaptic enrichment of GluD1 — an orphan glutamate receptor with emerging roles in synapse stabilization and modulation — suggests a potential organizing role in the postsynaptic apparatus, possibly gating the integration of fast and slow synaptic inputs.

Notably, the preferential targeting of PKCδ-expressing neurons places this novel synapse at the center of a highly investigated microcircuit involved in fear, anxiety, and homeostatic regulation. Previous work has implicated PKCδ+ CeC neurons as critical intermediates between brainstem-derived sensory inputs and downstream hypothalamic and brainstem effectors. The

discovery of a calyceal-type input to these neurons suggests a specialized pathway for high-throughput delivery of multimodal signals, capable of driving immediate behavioral responses while simultaneously engaging modulatory systems.

From a systems perspective, this dual-modality synapse could serve as a hub for integrating viscerosensory, nociceptive, and affective information — domains in which PACAP, CGRP, and neurotensin are individually known to operate. The PACAP-induced enhancement of PKCδ neuron excitability observed in our recordings further supports the functional relevance of this input, hinting at a role in amplifying or prolonging responses to stress or internal bodily states.

In sum, our findings reveal a previously unrecognized synaptic architecture in the extended amygdala, merging structural specializations of calyceal transmission with a chemically diverse synaptic profile. This convergence may represent an evolutionarily conserved mechanism for integrating and prioritizing homeostatically relevant inputs in the context of emotional and behavioral control. Future work will be needed to define the afferent origin of these terminals, dissect their behavioral relevance, and explore their potential plasticity under conditions of chronic stress or pathology

Material and methods

Animals

Rats

Adult (>60 days) male Wistar rats were obtained from the vivarium of the School of Medicine of the National Autonomous University of Mexico. Rats were housed in humidity and temperature-controlled vivarium using a normal light cycle with lights on at 7:00 hours and lights off at 19:00 hours. Animals had ad-libitum access to standard laboratory chow and water. All procedures were approved by the Ethics committee of the School of Medicine, of the National Autonomous University of Mexico, license number CIEFM-079-2020.

Mice

Adult (>postnatal day 60) male and female C57/Bl6J WT, PKC-delta (Protein Kinase C delta) -Ai9 (PKCδ-Ai9), were used. Mice were housed in humidity and temperature-controlled vivariums using a normal light cycle with lights on at 7:00 hours and lights off at 19:00 hours. Animals had ad-libitum access to standard laboratory chow and water. All procedures were approved by the National Institute of Mental Health Animal Care and Use Committee, NIMH/ACUC approval LCMR-08.

Immunohistochemistry for light microscopy

Rodents were perfused via the ascending aorta with 0.9% NaCl at room temperature, followed by 4% paraformaldehyde. Brain slices (70 µm) were obtained using a vibratome (Leica VT1200). Slices were washed 3 times in PB, blocked in TBST (Trisma Buffer 0.05M, NaCl 0.9%, 0.3% Triton-X) plus 10% Normal Donkey serum for 2 hrs. Slices were then incubated overnight at 4°C with

the following primary antibodies: rabbit anti PACAP (1:2000, BMA, T-4473), guinea pig anti VGLUT1 (1:5000, Chemicon, AB-5905), mouse anti VGLUT2 (1:1000, Chemicon, MAB-5504), guinea pig anti VGLUT2 (1:2000, SySy, 135 404), rabbit anti VAChT (produced and provided by Dr. Lee Eiden, NIMH, NIH), rabbit anti CGRP (1:1000, Phoenix, H-015-09), mouse anti neurotensin (1:1000, Sigma, SAB-4200703), goat anti calretinin (1:2000, Swant, CG1), diluted in TBST plus 1% NDS. The next day slices were thoroughly washed 3 times in TBST and incubated during two hours in the appropiate secondary biotinylated or fluorescent antibodies from Vector Labs at a concentration of 1:500. The processed sections were examined under bright field using a Nikon Eclipse E600 microscope along with its digital camera for photographic documentation and immunofluorescent reactions were observed using a Stellaris Confocal Microscope from Leica Microsystems.

Ex-vivo whole-cell electrophysiology

Ai9-TdTomato-PKCδ mice were used for this study. Anesthesia was induced with pentobarbital, and mice were subsequently decapitated. Brains were rapidly removed and immersed in an ice-cold cutting solution containing (in mM): 92 NMDG, 20 HEPES, 25 glucose, 30 $NaHCO_3$, 2.5 KCl, 1.2 NaH_2PO_4, 10 $MgSO_4$, and 0.5 $CaCl_2$, saturated with 95% O_2/5% CO_2, with an osmolarity of 303–306 mOsm. Following extraction, brains were blocked and mounted in the specimen chamber of a Leica VT1200 vibratome filled with ice-cold cutting solution. Horizontal slices (300 µm thick) containing the central amygdala were sectioned. Slices were then incubated in the same cutting solution at 34°C for 5 minutes. Subsequently, slices were transferred to a chamber containing a holding aCSF solution composed of (in mM): 92 NaCl, 20 HEPES, 25 glucose, 30 $NaHCO_3$, 2.5 KCl, 1.2 NaH_2PO_4, 1 $MgSO_4$, and 2 $CaCl_2$ (303–306 mOsm), saturated with 95% O_2/5% CO_2, and maintained at room temperature for at least 1 hour. Slices remained in this solution until transferred to the recording chamber.

For whole-cell recordings of intrinsic excitability, glass microelectrodes (3–5 MΩ) were filled with an internal solution containing (in mM): 135 K-gluconate, 10 HEPES, 4 KCl, 4 Mg-ATP, 0.3 Na-GTP, and 0.2% biocytin. The capsular region of the central amygdala was identified under low magnification using brightfield and fluorescence illumination. Neurons for recording were selected at high magnification using differential interference contrast (DIC) optics. After achieving whole-cell access and stabilization under voltage clamp, the configuration was switched to current clamp. Series resistance (<20 MΩ) was continuously monitored by measuring the response to a -40 pA current injection. Cells exhibiting a >20% change in series resistance during the recording were excluded from further analysis. Recordings were obtained using a Multiclamp 700B amplifier (Molecular Devices), filtered at 2 kHz, and digitized at 20 kHz with a Digidata 1440A Digitizer (Molecular Devices).

PACAP Application to Brain Slices: to assess the intrinsic excitability of Ai9-PKCδ neurons under current clamp, a current injection protocol was applied, consisting of 1-second steps from -40 pA to 240 pA in 20 pA increments, with 7-second intervals between steps. This protocol was continuously repeated throughout the recording session. Three experimental conditions were

evaluated: (1) baseline perfusion with aCSF for 15 minutes, (2) application of aCSF containing 100 nM PACAP for 15 minutes, and (3) a washout period with standard aCSF. For each cell, five runs of the protocol in each condition were averaged. For each cell a two-way ANOVA was used to determine whether PACAP application significantly altered the current-induced firing rate. A total of 30 neurons from the capsular region of the central amygdala (CeA) were recorded. After recording, the sections were drop-fixed in 4% PFA in PB for subsequent developing with streptavidin-488 and immunocharacterization.

RNAscope

Brains were rapidly dissected, flash-frozen on dry ice, and stored at -80°C until sectioning for in situ hybridization (ISH). Coronal brain sections (16 µm thick) were obtained using a cryostat set to -20°C and mounted directly onto microscope slides. Slides containing ISH sections were stored at -80°C until further processing. RNAscope ISH was performed following the Advanced Cell Diagnostics (ACD) user manual and previously published protocols.

Briefly, slides were fixed in 10% neutral-buffered formalin for 20 minutes at 4°C, then washed twice with PBS for 1 minute each. This was followed by dehydration in 50% ethanol (5 min), 70% ethanol (5 min), and 100% ethanol (5 min), after which the slides were stored in 100% ethanol at -20°C overnight. The next day, slides were air-dried at room temperature (RT) for 10 minutes. A hydrophobic barrier was drawn around the tissue sections using a hydrophobic barrier pen and allowed to dry for 10–15 minutes at RT. Sections were then incubated with Protease IV solution for 20 minutes at RT, followed by two 1-minute washes in distilled water (ddH_2O). Slides were then incubated with the appropriate probes for 2 hours at 40°C in a HybEZ™ oven (Advanced Cell Diagnostics). The following probes were used (purchased from ACD): Mm-Grid1-C1 (Cat No. 552311, target region 396–1301; Accession No. NM_008166.2); Mm-Adcyap1r1-C2 (Cat No. 409561-C2, target region 4108–5038; Accession No. NM_001025372.1); Mm-Chrna7-C3 (Cat No. 465161-C3, target region 175–1122; Accession No. NM_007390.3). Following hybridization, slides were washed twice for 2 minutes each in wash buffer, then incubated sequentially with the corresponding amplification reagents in the HybEZ™ oven at 40°C. DAPI was applied for nuclear staining at room temperature for 20 seconds. Slides were then coverslipped and stored at 4°C until imaging. Confocal images were acquired using a Leica Stelaris confocal microscope with a 20x objective and four channels: DAPI, Alexa Fluor 488, Alexa Fluor 550, and Alexa Fluor 647

Statistics

For statistical analysis of the recorded cells, neurons were classified into two groups based on their response to 100 nM PACAP: responders (n = 21) and non-responders (n=9). To evaluate whether PACAP application produced a statistically significant effect, a two-way ANOVA was performed, with treatment condition (baseline, PACAP, and washout) as one factor and current step amplitude as the second factor. Statistics were computed using GraphPad Prism.

Transmission Electron Microscopy

Brains of C57BL WT mice were sectioned at 70 um with a Leica VT1000 vibratome, slices were rinsed with PB, incubated with 1% sodium borohydride in PB for 30 min to inactivate free aldehyde groups, rinsed in PB, and then incubated with blocking solution [1% normal goat serum (NGS), 4% BSA in PB supplemented with 0.02% saponin] for 30 min. Sections were then incubated with primary antibodies, as follows: Ms anti PKCδ 1:1000 (BD Trousduction Cat#610397); Rb anti PACAP (1:50, BMA Cat#T4473); Gp anti VAChT Japan (1:500, Frontier Institutes Cat#VAChT-Gp-Af1120); Gp anti VGluT1 (1:500, Frontier Institutes Cat# VGluT1-GP-Af570); Rb anti Dsred (1:1000, Clontech, Cat #: 632496); Gp anti VGluT2 (1:500, Frontier Institute Cat#VGluT2-GP-Af810); Rb anti GRID1 (1:100, Alomone Lab, Cat# AGC-038); Rb anti VGluT2 (1:500, Frontier Institute Cat#VGluT2-Rb-Af720-1); Rb anti VChAT (1:500, Frontier Institute, Cat#VAChT-Rb-Af670). All primary antibodies were diluted with 1% normal goat serum (NGS), 4% BSA in PB supplemented with 0.02% saponin and incubations were for 24 h at 4°C.
Sections were rinsed and incubated overnight at 4°C in the corresponding secondary antibodies: Nanogold anti Mouse, Fab (1:100, Nanoprobes, Cat#39C450); Nanogold anti Rb, Fab (1:100, Nanoprobes, Cat#39C881); Nanogold anti GP,Fab (1:100, Nanoprobes, Cat#06S099); Biotinylated anti mouse (1:100, Vector laboratory); Biotinylated anti Rb (1:100, Vector laboratory); Biotinylated anti Gp (1:100, Vector laboratory). Sections were rinsed in PB, and then incubated in avidin-biotinylated horseradish peroxidase complex in PB for 2 h at room temperature. Sections were rinsed in PB and postfixed with 1.5% glutaraldehyde at room temperature for 10 min. Sections were rinsed again in PB and in double-distilled water, followed by silver enhancement of the gold particles with the Nanoprobe Silver Kit (2012, Nanoprobes Inc.) for 7 min at room temperature. Next, peroxidase activity was detected with 0.025% 3,3'-diaminobenzidine (DAB) and 0.003% H2O2 in PB for 5-10 min. Sections were rinsed with PB and fixed with 0.5% osmium tetroxide in PB for 25 min, washed in PB, followed by double distilled water wash, and then contrasted in freshly prepared 1% uranyl acetate for 35 min. Sections were dehydrated through a series of graded alcohols and with propylene oxide, and were then flat embedded in Durcupan ACM epoxy resin (14040, Electron Microscopy Sciences, Hatfield, PA). Resin-embedded sections were polymerized at 60°C for 2 days, and sections of 60 nm were cut from the outer surface of the tissue with an ultramicrotome UC7 (Leica Microsystems, Deerfield, IL) using a diamond knife (Diatome, Hatfield, PA). The sections were collected on formvar-coated single slot grids and counterstained with Reynolds lead citrate to be examined and photographed using a Tecnai G2 12 transmission electron microscope (Fei Company, Hillsboro, OR) equipped with the OneView digital micrograph camera (Gatan, Pleasanton, CA).

Ultrastructural analysis. Serial ultrathin sections of the capsular region of the central amygdala (CeC) were analyzed. Synaptic contacts were classified according to their morphology and immunolabel and photographed at a magnification of 6,800- 13,000x. In the serial sections, a terminal containing more than 5 immunogold particles was considered as

immunopositive. Pictures were adjusted to match contrast and brightness by using Adobe Photoshop (Adobe Systems).

FIB-SEM Methodology:

To assess the three-dimensional anatomical characteristics of the Calix-like contacts, some slices processed immunohistochemistry against PACAP for Electron microscopy, were embedded in Durcupan resin, platinum-covered and positioned in a microscope sample holder. The electron image stack was collected using a ZEISS Crossbeam 550 FIB-SEM (Zeiss Group, Oberkochen, Germany), equipped with a high-performance field emission electron column and a gallium-ion beam column. The ion beam was accelerated at 30 kV for both rough and fine milling. A coarse trench was milled around the protective platinum (Pt) layer using a 15 nA ion current. To prevent curtain artifacts, a thin (~1 µm thick, covering an area of 10 × 10 µm) platinum protective layer was deposited on top of the catalytic layer by injecting a platinum precursor via the gas injection system, using the ion beam at 30 kV and 3 nA.
A chevron-patterned FIB milling registration mark was milled into the protective platinum pad, and an additional FIB-mediated carbon pad was deposited to create a fiducial mark. This allowed for precise control of the slice thickness and ensured accurate 3D alignment of the image stack, resulting in distortion-free reconstruction. These processes were controlled using ZEISS ATLAS 3D Nanotomography software.
The images were acquired using an Energy-selective Backscattered (EsB) detector with the EsB grid set to 1.5 kV. The SEM beam operated at an accelerating voltage of 3 kV and a current of 1.5 nA, which was optimized for sequential removal of thin slices during the nanotomography process. The total depth of the trench created by this procedure was 20 µm. Backscattered electron images were captured in the X-Y plane, while the sequential removal of slices occurred along the Z-axis. For tomography, a pixel size of 20 nm × 10 nm was used, corresponding to a slice thickness of 20 nm.
The raw FIB-SEM dataset comprised 1568 images, which were cropped and processed into a single volume image. The final volume image was reconstructed and analyzed and segmented using ORS Dragonfly software.

Funding:

- UNAM (México): PAPIIT-IG200121 (LZ & RAB)
- SECIHTI (México): CF-2023-G-243 (LZ, RAB, RH-P), CB-238744 (RAB)
- Intramural Research Program of the NIMH, NIH (USA) (ZIAMH002386, LEE)

References

Dai, J., C. Patzke, K. Liakath-Ali, E. Seigneur and T. C. Sudhof (2021). "GluD1 is a signal transduction device disguised as an ionotropic receptor." Nature **595**(7866): 261-265.
Daniel, S. E. and D. G. Rainnie (2016). "Stress Modulation of Opposing Circuits in the Bed Nucleus of the Stria Terminalis." Neuropsychopharmacology **41**(1): 103-125.

Dong, Y. L., Y. Fukazawa, W. Wang, N. Kamasawa and R. Shigemoto (2010). "Differential postsynaptic compartments in the laterocapsular division of the central nucleus of amygdala for afferents from the parabrachial nucleus and the basolateral nucleus in the rat." J Comp Neurol **518**(23): 4771-4791.
Harris, K. M. and R. J. Weinberg (2012). "Ultrastructure of synapses in the mammalian brain." Cold Spring Harb Perspect Biol **4**(5).
Held, H. (1893). "Die centrale Gehörleitung." Arch Anat Physiol Anat Abt,.
Jaramillo, A. A., J. A. Brown and D. G. Winder (2021). "Danger and distress: Parabrachial-extended amygdala circuits." Neuropharmacology **198**: 108757.
Liakath-Ali, K., J. S. Polepalli, S. J. Lee, J. F. Cloutier and T. C. Sudhof (2022). "Transsynaptic cerebellin 4-neogenin 1 signaling mediates LTP in the mouse dentate gyrus." Proc Natl Acad Sci U S A **119**(20): e2123421119.
Lorteije, J. A., S. I. Rusu, C. Kushmerick and J. G. Borst (2009). "Reliability and precision of the mouse calyx of Held synapse." J Neurosci **29**(44): 13770-13784.
Nakamura, P. A. and K. S. Cramer (2011). "Formation and maturation of the calyx of Held." Hear Res **276**(1-2): 70-78.
Radke, A. K. (2009). "The role of the bed nucleus of the stria terminalis in learning to fear." J Neurosci **29**(49): 15351-15352.
Satzler, K., L. F. Sohl, J. H. Bollmann, J. G. Borst, M. Frotscher, B. Sakmann and J. H. Lubke (2002). "Three-dimensional reconstruction of a calyx of Held and its postsynaptic principal neuron in the medial nucleus of the trapezoid body." J Neurosci **22**(24): 10567-10579.
Shimada, S., S. Shiosaka, P. C. Emson, C. J. Hillyard, S. Girgis, I. MacIntyre and M. Tohyama (1985). "Calcitonin gene-related peptidergic projection from the parabrachial area to the forebrain and diencephalon in the rat: an immunohistochemical analysis." Neuroscience **16**(3): 607-616.
Takeuchi, Y., Q. Xie, T. Miki, Y. Matsumoto, I. Satriotomo, H. P. Li and H. Gu (2004). "Parabrachial inputs to Fos-immunoreactive neurons in the lateral central nucleus of amygdala activated by hypotension: a light and electron microscopic study in the rat." Brain Res Bull **64**(2): 171-180.

Supplementary Information

Novel multi-transmitter calyx-like giant synapse revealed in the extended amygdala

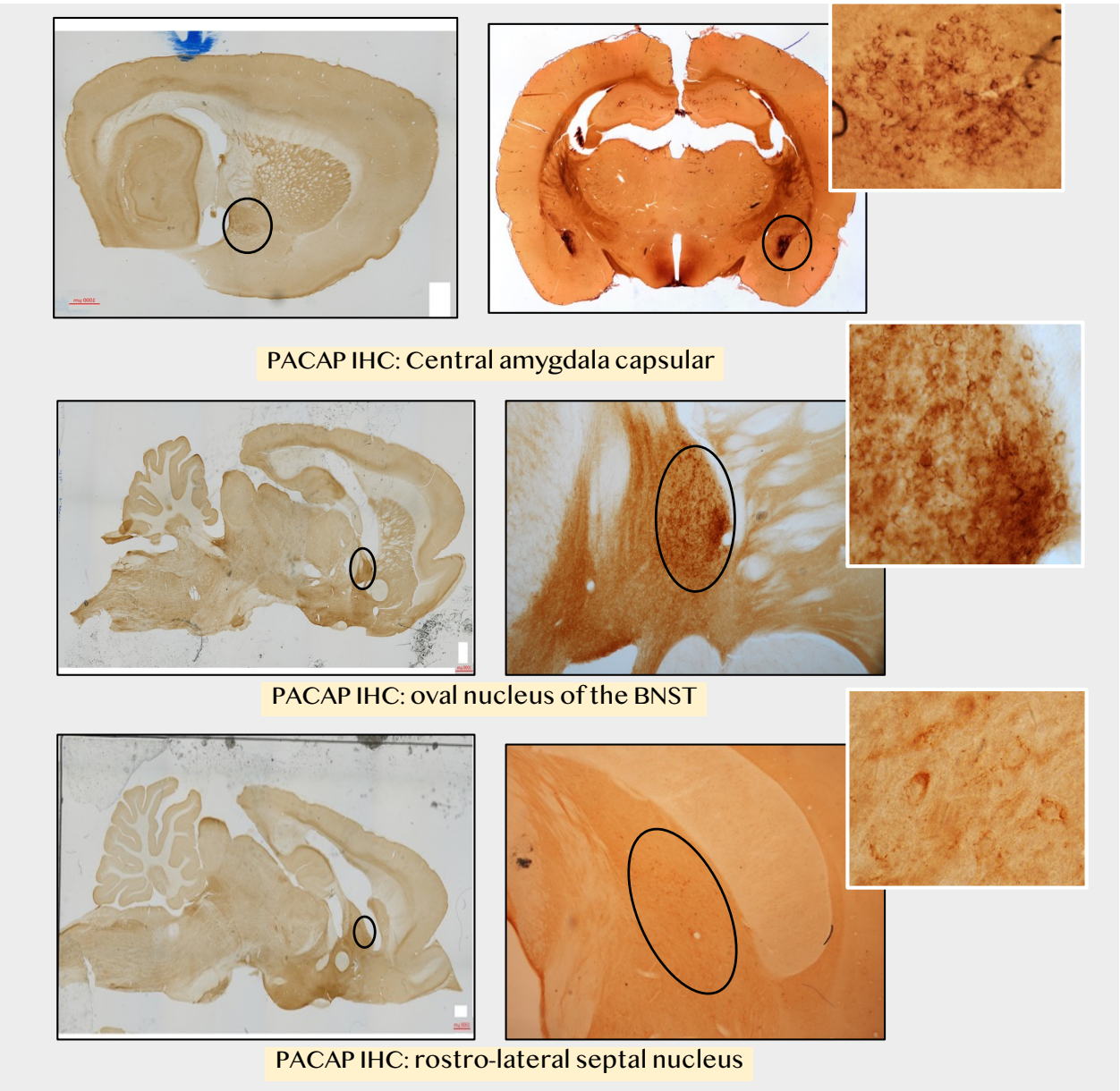

Supplement figure 1 to Figure 1 to Figure 1

Calyceal axonal endings in rat telencephalic structures observed PACAP